Since January 2020 Elsevier has created a COVID-19 resource centre with free information in English and Mandarin on the novel coronavirus COVID-19. The COVID-19 resource centre is hosted on Elsevier Connect, the company's public news and information website.

Clinica Chimica Acta 536 (2022) 6–11

Contents lists available at ScienceDirect

Clinica Chimica Acta

journal homepage: www.elsevier.com/locate/cca

Development of multiplex S-gene-targeted RT-PCR for rapid identification of SARS-CoV-2 variants by extended S-gene target failure

Yuri Imaizumi [a], Takayuki Ishige [a,*], Tatsuki Fujikawa [a], Akiko Miyabe [a], Shota Murata [a], Kenji Kawasaki [a], Motoi Nishimura [a], Toshibumi Taniguchi [b], Hidetoshi Igari [b], Kazuyuki Matsushita [a]

[a] Division of Laboratory Medicine, Chiba University Hospital, 1-8-1 Inohana, Chuo-ward, Chiba-city, Chiba 2608677, Japan
[b] Department of Infectious Disease, Chiba University Hospital, 1-8-1 Inohana, Chuo-ward, Chiba-city, Chiba 2608677, Japan

ARTICLE INFO

Keywords:
SARS-CoV-2
Variant of concern
S-gene target failure
Multiplex RT-PCR
Rapid screening

ABSTRACT

Background: Tracking SARS-CoV-2 variants of concern (VOC) by genomic sequencing is time-consuming. The rapid screening of VOCs is necessary for clinical laboratories. In this study, we developed a rapid screening method based on multiplex RT-PCR by extended S-gene target failure (eSGTF), a false negative result caused by S-gene mutations.

Methods: Three S-gene target (SGT) regions (SGT1, codons 65–72; SGT2, codons 152–159; and SGT3, codons 370–377) and an N-gene region (for internal control) were detected in single-tube. Four types of VOC (Alpha, Delta, Omicron BA.1, and Omicron BA.2) are classified by positive/negative patterns of 3 S-gene regions (eSGTF pattern).

Results: The eSGTF patterns of VOCs were as follows (SGT1, SGT2, SGT3; P, positive; N, negative): Alpha, NPP; Delta, PNP; Omicron BA.1, NPN pattern; and Omicron BA.2, PPN. As compared with the S-gene sequencing, eSGTF patterns were identical to the specific VOCs (concordance rate = 96.7%, N = 206/213). Seven samples with discordant results had a minor mutation in the probe binding region. The epidemics of VOCs estimated by eSGTF patterns were similar to those in Japan.

Conclusions: Multiplex RT-PCR and eSGTF patterns enable high-throughput screening of VOCs. It will be useful for the rapid determination of VOCs in clinical laboratories.

1. Introduction

Severe acute respiratory syndrome coronavirus 2 (SARS-CoV-2), which causes coronavirus disease 2019 (COVID-19), emerged at the end of 2019 and rapidly spread globally [1]. Various molecular diagnostic techniques, vaccines, and antiviral agents have been developed [2–4]. However, the number of COVID-19 patients has been increasing because of the prevalence of the variants of concern (VOC) such as Alpha, Delta, and Omicron, which increase transmissibility and escape vaccine-induced protection [5,6]. Genomic surveillance is important to investigate virus transmission dynamics, detect novel genetic variants, and assess the impact of mutations on the performance of molecular diagnostic methods, antiviral drugs, and vaccines.

Genomic sequencing is the gold standard to identify SARS-CoV-2 variants [7]. However, genomic sequencing is a labor-intensive and time-consuming technique that requires specific instrument and bioinformatic skills. Thus, a high-throughput and cost-effective method is critical for the rapid screening of VOC.

Each VOC has characteristic mutations in the S-gene which encodes the spike protein [8]. Recently, real-time PCR-based methods have been used to screen VOC [9,10]. The TaqMan probe-based endpoint genotyping methodologies for targeting specific mutations such as N501Y and L452R are commercially available. In addition, it has been reported that the S-gene target failure (SGTF), which is a false negative result caused by S-gene mutation, is a marker of the Alpha and Omicron BA.1 variant [11,12].

In this study, we developed a single-tube, rapid VOC screening assay based on multiplex RT-PCR for targeting 3 S-gene regions and 1N-gene region. Targeted S-gene regions were as follows: S-gene target 1 (SGT1), codons 65–72; SGT2, codons 152–159; and SGT3, codons 370–377. This

* Corresponding author at: Division of Laboratory Medicine, Chiba University Hospital, 1-8-1 Inohana, Chuo-word, Chiba-city, Chiba 2608677, Japan.
E-mail address: ishige-t@chiba-u.jp (T. Ishige).

https://doi.org/10.1016/j.cca.2022.08.031
Received 24 August 2022; Accepted 31 August 2022
Available online 14 September 2022

Table 1
Primers and probes used in this study.

ID	Sequence (5́–3́)	Position (NC_045512)	Size (bp)
SGT1-F	aattctttcacacgtggtgttt	21,650–21,671	163
SGT1-R	ggacagggttatcaaacctctta	21,790–21,812	
SGT1-P	[FAM]-ttccatgctatacatgtctctggg-[BHQ1]	21,755–21,777	
SGT2-F	gaagacccagtccctacttat	21,898–21,918	188
SGT2-R	aaggctgagagacatattcaaa	22,064–22,085	
SGT2-P	[HEX]-tggatggaaagtgagttcagagtt-[BHQ1]	22,019–22,044	
SGT3-F	ttagagtccaaccaacagaatcta	22,515–22,538	200
SGT3-R	aggagacactccataacactt	22,694–22,714	
SGT3-P	[TexasRed]-aattccgcatcattttccacttttt-[BHQ2]	22,669–22,692	
NIID-N2-F	aaattttggggaccaggaac	29,125–29,144	158
NIID-N2-R	tggcacctgtgtaggtcaac	29,263–29,282	
NIID-N2-P	[Cy5]-atgtcgcgcattggcatgga-[BHQ3]	29,222–29,241	

assay was designed to classify 4 types of VOCs (Alpha, Delta, Omicron BA.1, and Omicron BA.2) by the extended SGTF (eSGTF) patterns (positive/negative patterns in SGT1-3).

2. Material and methods

2.1. Specimens

471 SARS-CoV-2 RNA-positive samples were used from November 2020 to June 2022 at Chiba University Hospital. The SARS-CoV-2 RNA detection test was performed using the Ampdirect 2019-nCoV detection kit (Shimadzu, Kyoto, Japan). The viral RNA extraction was performed as described previously [13]. In the positive samples, 21 samples were excluded because of low viral RNA (less than 100 copies/μL, approximately Cq > 30). Thus, 450 samples were analyzed.

2.2. RT-PCR

A Cobas z 480 instrument (Roche Diagnostics, Mannheim, Germany) was used for the RT-PCR. Before genotyping, a color compensation experiment was performed according to the manufacturer's instructions. The filter combinations for fluorescence detection (excitation-emission) were as follows: 465–510 (FAM), 540–580 (HEX), 540–610 (TexasRed), and 610–670 (Cy5). Each 10 μL reaction mixture contained 2.5 μL of 4 × TaqPath 1-Step RT-qPCR Master Mix (No ROX; Thermo Fisher Scientific, Waltham, MA, USA), 1 μL of 10 × Primer mixture (including 2 μM of primers and 1 μM of probes, Table 1), 1 μL of RNA sample and 5.5 μL of nuclease-free water. The NIID-N2 primer set was included as an internal control of SARS-CoV-2 RNA detection [14]. The final concentrations of primers and probes were 0.2 μM (primers) and 0.1 μM (probes). The Cq values were determined by the manual Fit Points method. The viral RNA concentrations were quantified by using EDX SARS-CoV-2 Standard (200 copies/μL; Bio-Rad, Hercules, CA, USA). The assay quality was controlled by samples of each VOC determined by S-gene sequencing.

2.3. Determination of VOC by Sanger sequencing

The VOC was determined using the previously described long-range RT-PCR and Sanger sequencing [15].

3. Results

3.1. Primer design

Three SGT regions and targeted mutations in VOC are shown in Fig. 1. The targeted mutations of each SGT1-3 were as follows: SGT1, H69_V70del (Alpha, Omicron BA.1); SGT2, F157_R158del (Delta) and

Table 2
Sensitivity and PCR efficiency of each target of multiplex RT-PCR.

Copies	Statistics	Target			
		SGT1	SGT2	SGT3	NIID-N2
6.25	Cq (Mean)	31.7	32.2	32.2	33.1
	% Detection	100% (4/4)	100% (4/4)	100% (4/4)	100% (4/4)
12.5	Cq (Mean)	30.7	31.1	31.3	32.1
	% Detection	100% (4/4)	100% (4/4)	100% (4/4)	100% (4/4)
25	Cq (Mean)	29.8	30.1	30.3	31.0
	% Detection	100% (2/2)	100% (2/2)	100% (2/2)	100% (2/2)
50	Cq (Mean)	28.8	29.2	29.4	30.3
	% Detection	100% (2/2)	100% (2/2)	100% (2/2)	100% (2/2)
100	Cq (Mean)	27.8	28.1	28.3	29.3
	% Detection	100% (2/2)	100% (2/2)	100% (2/2)	100% (2/2)
200	Cq	26.8	27.1	27.4	28.2
	Slope	–3.261	–3.381	–3.187	–3.200
	% Efficiency	103%	98%	106%	105%

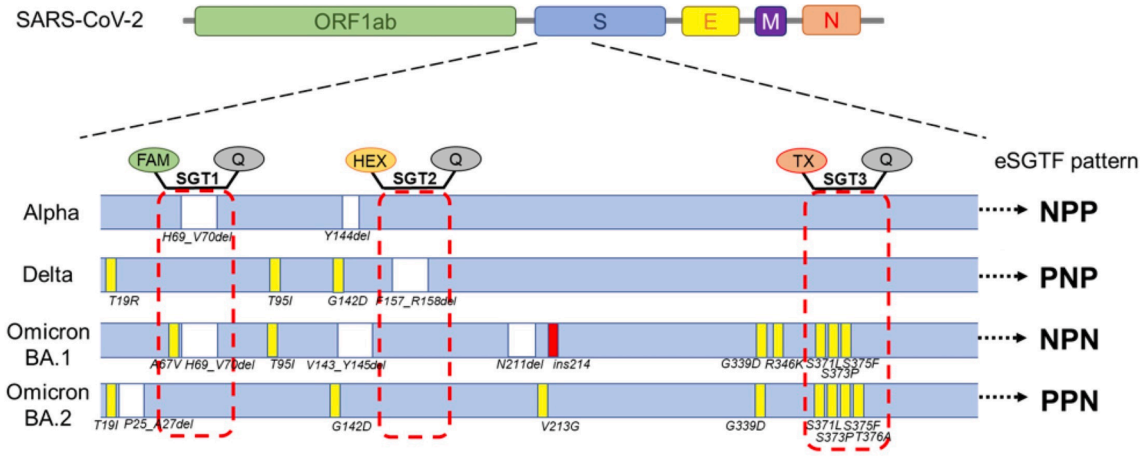

Fig. 1. Schematic representation of S-gene target regions in multiplex RT-PCR. The mutational positions in VOC are shown in white (deletion), yellow (substitution), and red (insertion) boxes. The SGT1, SGT2, and SGT3 target H69-V70del, F157-R158del and multiple substitutions in codons 371–376, respectively. The expected eSGTF pattens (SGT1/SGT2/SGT3; P, positive; N, Negative) of VOCs are as follows: Alpha, NPP; Delta, PNP; Omicron BA.1, NPN; and Omicron BA.2, PPN.

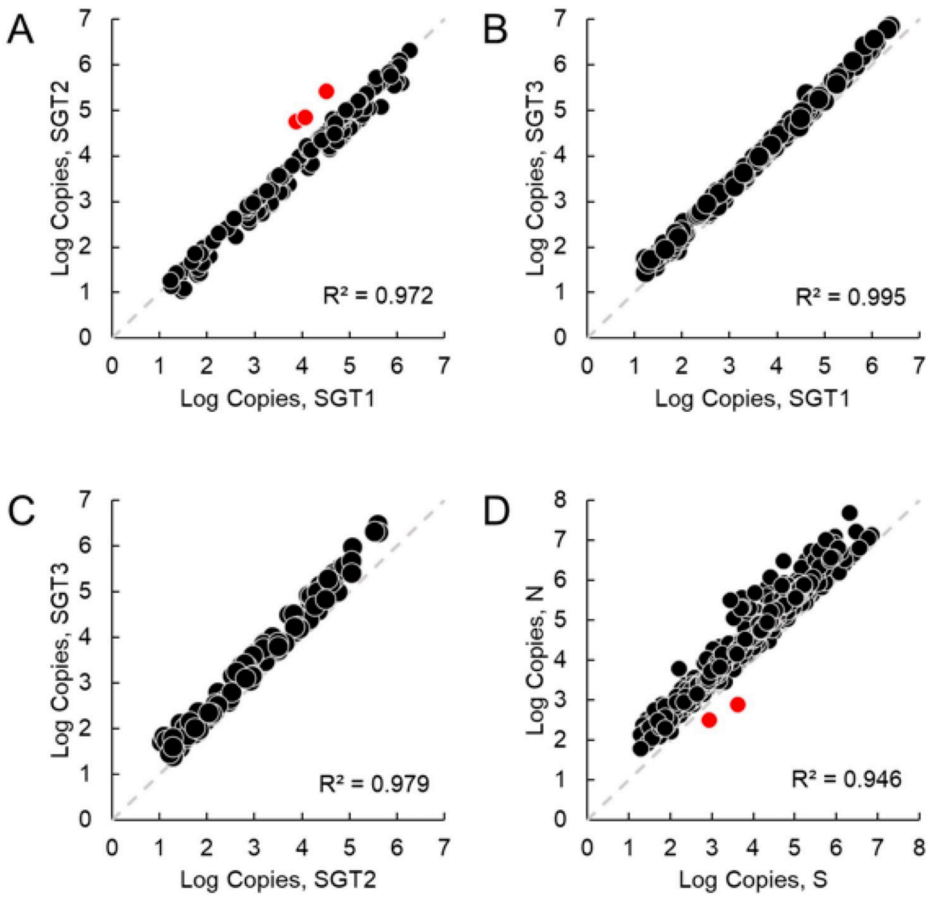

Fig. 2. Comparison of the viral RNA concentration (log copies) in each target: [A] SGT1 and SGT2 (N = 163); [B] SGT1 and SGT3 (N = 143); [C] SGT2 and SGT3 (N = 98); and [D] N-gene and S-gene (N = 450). The maximum value of SGT1-3 was used as S-gene RNA concentration. The outlier data is indicated in red points.

Table 3
Unexpected mutations in primer/probe regions detected in this study. The mismatched nucleotides in primer/probe regions are highlighted in bold upper cases. The primer/probe sequences are as follows: SGT1-F, aattctttcacacgtggtgttt; SGT2-P, tggatggaaagtgagttcagagtt; and NIID-N2-F, aaattttggggaccaggaac.

Mutation	Region	Sequence alteration	Observed effect
C21658T (Silent)	SGT1-F	aattctttTacacgtggtgttt	Increased Cq
G22017T (S:W152L)	SGT2-P	tTgatggaaagtgagttcagagtt	Decreased signal
G22017T (S:W152L) &G22026A (S:S155N)	SGT2-P	tTgatggaaaAtgagttcagagtt	Target failure
C22033A (S:F157L)	SGT2-P	tggatggaaagtgagttAagagtt	Target failure
C29144T (Silent)	NIID-N2-F	aaattttggggaccaggaaT	Increased Cq

SGT3, multiple substitutions in codons 371–376 (Omicron BA.1 and BA.2). Four types of VOC were estimated by positive/negative patterns of SGT1-3(eSGTF patterns) as follows: Alpha, NPP pattern (SGT1 negative/SGT2 positive/SGT3 positive); Delta, PNP pattern (SGT1 positive/SGT2 negative/SGT3 positive); Omicron BA.1, NPN pattern (SGT1 negative/SGT2 positive/SGT3 negative); and Omicron BA.2, PPN pattern (SGT1 positive/SGT2 positive/SGT3 negative).

3.2. Sensitivity of multiplex RT-PCR

The sensitivity was analyzed using serially diluted EDX SARS-CoV-2 Standard samples (200, 100, 50, 25, 12.5, and 6.25 copies/μL). The Cq values, detection rates, slope, and PCR efficiency are shown in Table 2. SGT1-3 and NIID-N2 can detect 6.25 copies/μL and each PCR efficiency was between 98% and 106%.

3.3. Comparison of each target

The calculated SARS-CoV-2 RNA concentration of each SGT target was compared (Fig. 2A–C). Significant correlations were observed (R-squared values of 0.972–0.995). Although the SGT1 and SGT2 concentrations were almost equivalent, there were three samples that had lower SGT1 values than SGT2 (Fig. 2A). These three samples were Omicron BA.1 and have the silent mutation (C21658T) in the middle region of the SGT1 forward primer binding site (Table 3).

In addition, S-gene and N-gene concentrations were also compared (Fig. 2D). The maximum values of SGT1-3 were used as the S-gene concentration. The R-squared value was 0.946. N-gene concentrations were on average 4.7 times higher than the S-gene. There were two samples that had lower N-gene concentrations than the S-gene (Fig. 2D). These samples have the C29144T mutation, which was located at the 3́-end of the NIID-N2 forward primer binding site (Table 3).

3.4. Classification by eSGTF pattern

As a result, 449 samples were classified into the following seven clusters by the endpoint genotyping (Fig. 3): PPP, SGT1 positive/SGT2 positive/SGT3 positive; PwPP, SGT1 positive/SGT2 weak positive/SGT3 positive; NPP, SGT1 negative/SGT2 positive/SGT3 positive; PNP, SGT1 positive/SGT2 negative/SGT3 positive; NPN, SGT1 negative/SGT2 positive/SGT3 negative; PPN, SGT1 positive/SGT2 positive/SGT3 negative; and PNN, SGT1 positive/SGT2 negative/SGT3 negative. In the

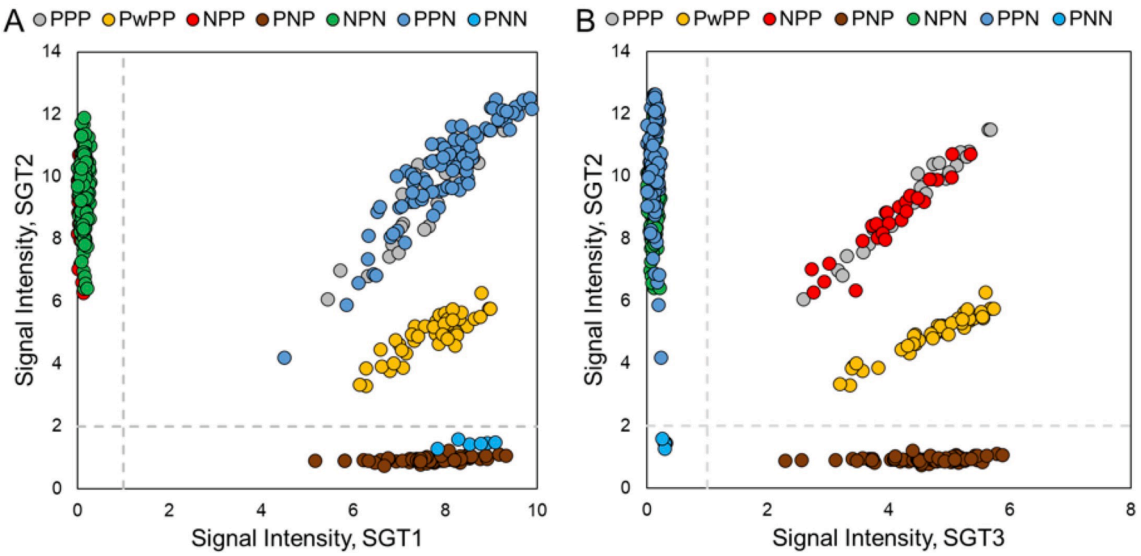

Fig. 3. The endpoint genotyping of SGT1–3. [A] SGT1 (x-axis) vs. SGT2 (y-axis). [B] SGT3 (x-axis) vs. SGT2 (y-axis). The sub-cluster, PwPP pattern which had low signal intensity of SGT2, was observed in PPP pattern (indicated yellow points). Dotted lines indicate threshold lines of positive/negative results. Numbers of samples are PPP (N = 26), PwPP (N = 46), NPP (N = 26), PNP (N = 71), NPN (N = 184), PPN (N = 91), and PNN (N = 6).

	Detected eSGTF Pattern								
Lineage	PPP	PwPP	NPP	PNP	NPN	PPN	PNN	NNP	NNN
Unclassified	**21**	0	0	0	0	0	0	0	0
R.1	0	**41**	0	**1**	0	0	0	0	0
Alpha	0	0	**17**	0	0	0	0	0	0
Delta	0	0	0	**57**	0	0	0	0	0
Omicron BA.1	0	0	0	0	**46**	0	0	0	0
Omicron BA.2	0	0	0	0	0	**24**	**6**	0	0

Fig. 4. Comparison of sequencing results and eSGTF patterns. The lineages were determined by entire S-gene sequencing (N = 213). The concordant and discordant results are highlighted in gray boxes and red letters, respectively.

PPP pattern, there was a sub-cluster, the PwPP pattern, which had a slightly decreased signal intensity of SGT2.

Compared with the S-gene sequencing, eSGTF patterns were identical to the specific VOCs (concordance rate = 96.7%, N = 206/213, Fig. 4). The PwPP pattern was identical to the R.1 lineage, which had a W152L mutation located in the SGT2 probe binding region (Table 3). Discordant results were observed in seven samples (1 sample of R.1 and 6 samples of Omicron BA.2). There was a sample of R.1 lineage with the PFP pattern, which was detected before the epidemic season of the Delta lineage. As a result of sequencing, this sample had S155N in addition to W152L mutations in the SGT2 probe binding region (Table 3). The PFF pattern was observed in six samples of Omicron BA.2. Although the signal intensity of SGT2 was slightly higher than the baseline (no-template control), we could not determine this signal as positive. By Sanger sequencing, the F157L mutation in the SGT2 probe binding region was detected in all six samples (Table 3).

3.5. *Time-to-time analysis of eSGTF patterns*

A result of time-to-time analysis is shown in Fig. 5. The PwPP (R.1), FPP (Alpha), and PFP (Delta) patterns were dominant in 3rd, 4th, and 5th waves, respectively. Then, the eSGTF patterns were shifted from FPF (Omicron BA.1) to PPF (Omicron BA.2) in 6th wave.

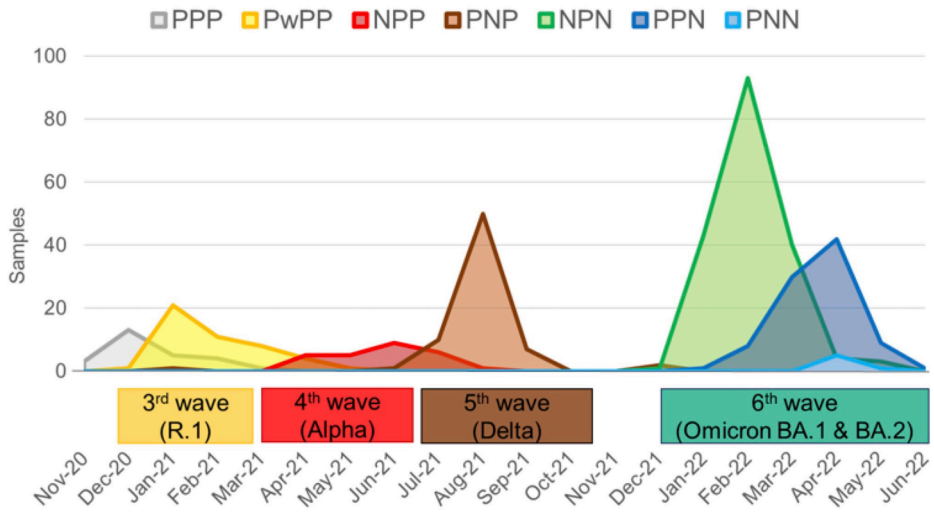

Fig. 5. Time-to-time analysis of eSGTF patterns in our laboratory.

4. Discussion

The multiplex RT-PCR we developed in this study could clearly classify four types of VOCs (Alpha, Delta, Omicron BA.1, and Omicron BA.2) by eSGTF patterns. The epidemics of these VOCs in our laboratory were similar to those in Japan [8]. Therefore, this method enables the simultaneous determination of mutational profiles in the 3 S-gene regions in a single-tube assay and able to determine VOCs in minimum 2 h from first detection.

Compared with the traditional TaqMan probe genotyping assay, the advantages of our method are a simple probe design and multiplex capability. Our method targeted 3 S-gene regions occurring deletions (H69_V70del and F157_R158del) and multiple substitutions (codons 371–376). These mutations strongly affected the binding affinity of probes and resulted in the target failure. Thus, modifications such as MGB and LNA were not required for mismatch discrimination (these modifications are frequently used to improve mismatch discrimination when detecting single nucleotide substitutions) [16,17]. Generally, the TaqMan probe genotyping assay detects one mutation using different fluorescent labeling probes, e.g., FAM-labeled wild-type specific probe and VIC-labeled mutant-type specific probe [18]. Many fluorescent filter combinations will be required for a multiplex assay in traditional TaqMan probe genotyping.

There were five types of mismatches, which affected the amplification efficiency and signal intensity, in primer or probe regions that were observed in this study (Table 3). The mismatches in primer regions caused a decrease in the amplification efficiency and resulted in an underestimation of the viral RNA concentration, especially the C29144T mutation in N-gene which was in the 3́-end of the forward primer binding region. A perfect match of the 3́-end of primer is important for the effective amplification of PCR. The decreased sensitivity of the C29144T mutation was also reported by the National Institute of Infectious Disease (NIID), Japan, which developed the NIID-N2 primer set used in this study [19]. The mismatches in the probe regions affected the signal intensity. These mismatches were frequently observed in the SGT2 probe region in this study. The W152L, S155N, and F157L mutations were in the 5́-region, middle, and 3́-region of the SGT2 probe binding site, respectively. It was thought that the binding affinity of the SGT2 probe was decreased by these mutations and resulted in the lower signal intensities or target failure of SGT2. Notably, the sample with both W152L and S155N mutations, which was R.1 lineage, had a completely negative signal because of the two mutations in the SGT2 probe region. Taken together, we speculate that Omicron BA.5 (with H69-V70del) and Omicron BA.2.75 (with W152R and F157L) may show NPN and PNN patterns of eSGTF, respectively [8].

It has been reported that SARS-CoV-2 has various sub-genome RNAs (sgRNA) [20,21]. The abundance of the N-gene region is higher than the other because canonical sgRNAs include the N-gene region [22]. Our results also indicated that N-gene abundance was higher than S-gene (Fig. 2D). Thus, the viral RNA concentrations in this study might be affected by sgRNAs.

There were some limitations in this study. First, it required sequencing to identify mutations when an unexpected eSGTF pattern is observed. Second, other VOCs, such as Beta and Gamma, may not be able to identify by our method, because there are no mutations in probe binding regions of S-gene (These VOCs may indicate PPP pattern). However, Beta and Gamma did not spread worldwide. Third, the current method will not be able to classify Omicron BA.1 and BA.5 since the same eSGTF pattern is expected. The additional mutation screening assay, e.g. L452R, will be required for separating BA.1 and BA.5. Finally, our approach cannot classify some recombinant variants because only S-gene mutations are targeted (XE vs. BA.2 and XF vs. BA.1) [23].

In conclusion, current multiplex RT-PCR and eSGTF patterns enable high-throughput VOC screening. This method is an easy-to-use and cost-effective methodology that will be useful to determine VOCs in clinical laboratories rapidly.

Author contributions

YI: Investigation, Writing – Original Draft. TI: Conceptualization, Investigation, Writing – Review & Editing. TF: Investigation. AM: Investigation. SM: Investigation. KK: Supervision. MN: Supervision. TT: Resources, Supervision. HI: Resources, Supervision, Project administration. KM: Writing – Review & Editing, Supervision, Project administration.

Declaration of Competing Interest

The authors declare that they have no known competing financial interests or personal relationships that could have appeared to influence the work reported in this paper.

References

[1] World Health Organization (WHO), WHO Coronavirus (COVID-19) Dashboard, 2021. <https://covid19.who.int> (Accessed 1 August 2022).
[2] I. Smyrlaki, M. Ekman, A. Lentini, N. Rufino de Sousa, N. Papanicolaou, M. Vondracek, J. Aarum, H. Safari, S. Muradrasoli, A.G. Rothfuchs, J. Albert, B. Högberg, B. Reinius, Massive and rapid COVID-19 testing is feasible by extraction-free SARS-CoV-2 RT-PCR, Nat. Commun. 11 (2020) 4812.
[3] F. Krammer, SARS-CoV-2 vaccines in development, Nature. 586 (2020) 516–527.
[4] L. Riva, S. Yuan, X. Yin, L. Martin-Sancho, N. Matsunaga, L. Pache, S. Burgstaller-Muehlbacher, P.D. De Jesus, P. Teriete, M.V. Hull, M.W. Chang, J.-W. Chan, J. Cao, V.-M. Poon, K.M. Herbert, K. Cheng, T.-T. Nguyen, A. Rubanov, Y. Pu, C. Nguyen, A. Choi, R. Rathnasinghe, M. Schotsaert, L. Miorin, M. Dejosez, T.P. Zwaka, K.-Y. Sit, L. Martinez-Sobrido, W.-C. Liu, K.M. White, M.E. Chapman, E.K. Lendy, R. J. Glynne, R. Albrecht, E. Ruppin, A.D. Mesecar, J.R. Johnson, C. Benner, R. Sun, P. G. Schultz, A.I. Su, A. García-Sastre, A.K. Chatterjee, K.-Y. Yuen, S.K. Chanda, Discovery of SARS-CoV-2 antiviral drugs through large-scale compound repurposing, Nature. 586 (7827) (2020) 113–119.
[5] W.T. Harvey, A.M. Carabelli, B. Jackson, R.K. Gupta, E.C. Thomson, E.M. Harrison, C. Ludden, R. Reeve, A. Rambaut, S.J. Peacock, D.L. Robertson, SARS-CoV-2 variants, spike mutations and immune escape, Nat. Rev. Microbiol. 19 (7) (2021) 409–424.
[6] S. Xia, L. Wang, Y. Zhu, L. Lu, S. Jiang, Origin, virological features, immune evasion and intervention of SARS-CoV-2 Omicron sublineages, Signal Transduct. Target Ther. 7 (2022) 241.
[7] World Health Organization, Genomic sequencing of SARS-CoV-2: a guide to implementation for maximum impact on public health, 8 January 2021, World Health Organization, 2021 https://apps.who.int/iris/handle/10665/338480.
[8] Outbreak info, Linage Comparison. <https://outbreak.info/compare-lineages> (Accessed 1 August 2022).
[9] P. Neopane, J. Nypaver, R. Shrestha, S.S. Beqaj, SARS-CoV-2 variants detection using TaqMan SARS-CoV-2 mutation panel molecular genotyping assays, Infect. Drug Resist. 14 (2021) 4471–4479.
[10] R.J. Dikdan, S.A.E. Marras, A.P. Field, A. Brownlee, A. Cironi, D.A. Hill, S. Tyagi, Multiplex PCR assays for identifying all major severe acute respiratory syndrome coronavirus 2 variants, J. Mol. Diagn. 24 (4) (2022) 309–319.
[11] A. Bal, G. Destras, A. Gaymard, K. Stefic, J. Marlet, S. Eymieux, H. Regue, Q. Semanas, C. d'Aubarede, G. Billaud, F. Laurent, C. Gonzalez, Y. Mekki, M. Valette, M. Bouscambert, C. Gaudy-Graffin, B. Lina, F. Morfin, L. Josset, COVID-Diagnosis HCL Study Group, Two-step strategy for the identification of SARS-CoV-2 variant of concern 202012/01 and other variants with spike deletion H69–V70, France, August to December 2020, Euro Surveill. 26 (2021) 2100008.
[12] R.S. Paton, C.E. Overton, T. Ward, The rapid replacement of the SARS-CoV-2 Delta variant by Omicron (B.1.1.529) in England, Sci. Transl. Med. 14 (2022) eabo5395.
[13] T. Ishige, S. Murata, T. Taniguchi, A. Miyabe, K. Kitamura, K. Kawasaki, M. Nishimura, H. Igari, K. Matsushita, Highly sensitive detection of SARS-CoV-2 RNA by multiplex rRT-PCR for molecular diagnosis of COVID-19 by clinical laboratories, Clin. Chim. Acta. 507 (2020) 139–142.
[14] K. Shirato, N. Nao, H. Katano, I. Takayama, S. Saito, F. Kato, H. Katoh, M. Sakata, Y. Nakatsu, Y. Mori, T. Kageyama, S. Matsuyama, M. Takeda, Development of genetic diagnostic methods for detection for novel coronavirus 2019 (nCoV-2019) in Japan, Jpn. J. Infect. Dis. 73 (2020) 304–307.
[15] M. Matsubara, Y. Imaizumi, T. Fujikawa, T. Ishige, M. Nishimura, A. Miyabe, S. Murata, K. Kawasaki, T. Taniguchi, H. Igari, K. Matsushita, Tracking SARS-CoV-2 variants by entire S-gene analysis using long-range RT-PCR and Sanger sequencing, Clin. Chim. Acta. 530 (2022) 94–98.
[16] I.V. Kutyavin, I.A. Afonina, A. Mills, V.V. Gorn, E.A. Lukhtanov, E.S. Belousov, M. J. Singer, D.K. Walburger, S.G. Lokhov, A.A. Gall, R. Dempcy, M.W. Reed, R. B. Meyer, J. Hedgpeth, 3'-minor groove binder-DNA probes increase sequence specificity at PCR extension temperatures, Nucleic Acids Res. 28 (2000) 655–661.
[17] D. Latorra, K. Arar, J. Michael Hurley, Design considerations and effects of LNA in PCR primers, Mol. Cell Probes. 17 (5) (2003) 253–259.
[18] S. Kim, A. Misra, SNP genotyping: technologies and biomedical applications, Annu. Rev. Biomed. Eng. 9 (1) (2007) 289–320.
[19] K. Shirato, Y. Tomita, H. Katoh, S. Yamada, S. Fukushi, S. Matsuyama, M. Takeda, Performance evaluation of real-time RT-PCR assays for the detection of severe

acute respiratory syndrome coronavirus-2 developed by the national institute of infectious diseases, Japan, Jpn. J. Infect. Dis. 74 (5) (2021) 465–472.
[20] S. Alexandersen, A. Chamings, T.R. Bhatta, SARS-CoV-2 genomic and subgenomic RNAs in diagnostic samples are not an indicator of active replication, Nat. Commun. 11 (2020) 6059.
[21] D. Kim, J.-Y. Lee, J.-S. Yang, J.W. Kim, V.N. Kim, H. Chang, The architecture of SARS-CoV-2 transcriptome, Cell. 181 (4) (2020) 914–921.e10.
[22] Z. Chen, R.W.Y. Ng, G. Lui, L. Ling, C. Chow, A.C.M. Yeung, S.S. Boon, M.H. Wang, K.C.C. Chan, R.W.Y. Chan, D.S.C. Hui, P.K.S. Chan, Y.Y. Go, Profiling of SARS-CoV-2 subgenomic RNAs in clinical specimens, Microbiol. Spectr. 10 (2) (2022) e0018222.
[23] L. Wang, H.-Y. Zhou, J.-Y. Li, Y.-X. Cheng, S. Zhang, S. Aliyari, A. Wu, G. Cheng, Potential intervariant and intravariant recombination of delta and omicron variants, J. Med. Virol. 94 (10) (2022) 4830–4838.